INTERNAL REPORT

STRESS ANALYSES FOR NUMERICAL MODELLING OF SUBMARINE FLOWSLIDES

by Harald Norem and
Bonsak Schieldrop

522090-10 28 FEBRUARY 1991

INTERNAL REPORT

STRESS ANALYSES FOR NUMERICAL MODELLING OF SUBMARINE FLOWSLIDES

by Harald Norem and Bonsak Schieldrop

522090-10 5 APRIL 1991

S U M M A R Y

This report is based on, and is a continuation of the NGI-report 522090-2 "An Approach to the Physics and the Modelling of Submarine Flowslides", by Norem, Locat and Schieldrop (1989).

Submarine flowslides are assumed to consist of two flow layers, a dense flow close to the bed and a turbidity current above that. Both reports concentrate on the dense part which is considered to behave as a granular material where visco-plastic behaviour is predominant. The present report establishes the assumptions and equations for the non-steady flow necessary for physical and numerical modelling of submarine flowslides. The equations developed are the momentum equation, the continuity equation with the corresponding boundary condition, as well as assumptions for the conditions at the upper and lower boundaries are presented.

The boundary stresses at the upper surface are assumed to be comparable with the stresses in the turbulent boundary layer along a flat plate. The shear stresses have their maximum at the front of the slide and are reduced to an almost constant level towards the rear.

The boundary conditions at the bed are assumed to be dependent on the roughness and the shear strength of the bed material. A non-slip velocity is assumed to exist for real slides, but may develop in model experiments with a smooth bed. On the other hand erosion may be significant if the bed consists of a soft material having a low shear strength. Equations to calculate the development of the slip velocity or the erosion depth are presented.

C O N T E N T S

1. INTRODUCTION

The aim of this report is to establish assumptions and expressions needed for physical and numerical modelling of submarine flowslides. The work is based on, and is a continuation of the NGI-report 522090-2 "An approach to the physics and the modelling of submarine flowslides" (Norem et al., 1989). The NGI-report was based on theories developed for the flow of granular materials, mainly snow avalanches, and established the main similarities and differences between snow avalanches and submarine flowslides. That report also presented the results originating from the application of the numerical model, originally developed for snow avalanches for the analysis of submarine slides.

The main aim of the present paper has been to establish the equations for non-steady flow, and to present reasonable assumptions for the boundary conditions of the dense flow. This will make it possible to reprogram the snow avalanche model to adapt it to submarine flowslides, or to develop a new numerical model for such slides.

2. A MATERIAL MODEL FOR THE DENSE PART OF SUBMARINE FLOW SLIDES

2.1 The constitutive equations

A general set of constitutive equations to describe the behaviour of granular flow was presented by Norem, Schieldrop and Irgens (1987, 1989) and Irgens (1988). This model assumes that granular materials may be treated as a continuum where visco-plastic behaviour is predominant. The model was originally made for snow avalanches, but has later also been adopted to submarine flowslides by Norem, Locat and Schieldrop (1989).

The model by Norem et al (1987) represents a modified CEF-fluid. (Criminale-Ericksen-Filbey, 1958), where the plasticity term is represented by generally accepted plasticity theory and the CEF-fluid represents the visco-elastic behaviour.

In a steady, simple shear flow the general constitutive equations in the model yields for the normal stresses, σ_x, σ_y, σ_z and the shear stresses, τ_{xy}, τ_{yz}, τ_{zx}, (Fig. 1):

$$\sigma_x = p_e + p_u - \left((\nu_1 - \nu_2)\, \bar{\rho}\, \frac{dv_x}{dy} \right)^r \tag{1}$$

$$\sigma_y = p_e + p_u + \bar{\rho}\nu_2 \left(\frac{dv_x}{dy} \right)^r \tag{2}$$

$$\sigma_z = p_e + p_u \; ; \quad \tau_{xz} = \tau_{yz} = 0 \tag{3}$$

$$\tau_{xy} = c + p_e \tan\varphi + \bar{m\rho} \left(\frac{dv_x}{dy} \right)^r \tag{4}$$

where c = cohesion

ϕ = friction angle

p_e = effective pressure (all normal compressive stresses have a positive sign according to soil mechanic practice)

p_u = pore water pressure

$\bar{\rho}$ = average density of the flowing material

m = shear stress viscosity of the flowing material

ν_1 and ν_2 = normal stress viscosities

r = exponent (assumed equal to 1 for submarine flow-slides)

2.2 Discussion of the parameters

The yield strength of the material is represented by the expression $c+p_e\tan\varphi$. The first term, c, is a pressure-independent parameter, which is zero for submarine flowslides consisting of sand or silt particles. The second term is a Coulomb friction dependent on the friction angle and the effective pressure.

The friction angle is according to Savage and Sayed (1984) and Hungr and Morgenstern (1984), very close to the internal static friction angle.

The effective pressure, p_e, is the pressure transferred through the grain lattice, and p_e can be found by Eq. 2. The main terms that define the magnitude of the effective pressure are the overburden, σ_y, the pore water pressure, p_u, and the dispersive pressure, $\bar{\rho}v_2(dv_x/dy)^r$.

The pore pressure plays a decisive part in the flow of submarine slides. It is thus a very important parameter to discuss and evaluate. The pore pressure may be seen as the sum of the following pressures, Fig. 2:

$$p_u = p_a + \rho_f g\,(H - y)\cos\alpha + \Delta u \rho_f g\,(h-y)\cos\alpha \qquad (5)$$

where p_a = the atmospheric pressure
Δu = the excess pore pressure expressed as the ratio to the hydrostatic pore pressure within the flowing mass
ρ_f = density of the interstitial fluid
H = height to the water level
h = height of the flowslide
g = acceleration of gravity
α = inclination of the slide path

Measurements of the pore pressure of materials liquiefied by blasting have shown that the pore pressure may have values 50% above the hydrostatic pressure (Kummeneje and Eide, 1961). Sassa (1988) made experiments with saturated sand exposed to a velocity gradient and found excess pore pressures inside the flowing mass increasing linearly up to 42% of hydrostatic pressure with increasing shear rates, and Hutchinson and Bhandari (1971) assumed the excess pore pressure to be dissipated according to the consolidation theory.

Edgers and Karlsrud (1982) investigated several submarine slides and found the run-out angle, the ratio of the vertical drop to the run-out distance, to vary within 1:200 and 1:10 (0.3^o - 5.7^o). This angle also reflects the maximum apparent friction angle of the sliding material, and such low values can be obtained only with high excess pore pressures. An angle of 2.3^o ($\tan\varphi = 0.04$) corresponds to a 90% reduction of the effective stress compared to the overburden effective stress, which is comparable to an excess pore pressure of 63%.

It is thus reasonable to assume that the initial excess pore pressure will be only slightly reduced during the flow, and the value of the

excess pore pressure will probably depend on both the shear rates (Sassa, 1988) and the particle size or permeability of the flowing material (Hutchinson, 1986).

The theoretical investigations on the dynamically induced stresses in flowing granular materials were initiated by Bagnold (1954). Due to interparticle contacts he found the existence of both a dispersive pressure in the y-direction $\tilde{\rho}\nu_2(dv_x/dy)^r$ and a dynamic shear stress $\tilde{\rho}m(dv_x/dy)^r$. The exponent, r, is equal to 1 in the macro-viscous regime and 2 in the inertia regime.

The ratio of the shear stress and the normal stress viscosities, m/ν_2, has been studied experimentally by Bagnold (1954) and Savage and Sayed (1984), and both have found the ratio to be a material constant. Bagnold (1954) assumed this ratio to be close to 0.75 in the macro-viscous regime, and Savage (1983) assumed the ratio to be dependent on the coefficient of restitution, and for sand the ratio lies between probably 0.6 and 0.7.

There are several experiments and theories on estimating the viscosity of granular materials in an interstitual fluid. Wildemuth and Williams (1985) found magnitudes of 10-500 times the viscosity of the interstitial fluid for volumetric densities between 0.45-0.70. These values are somewhat below those proposed by Bagnold (1954). Locat and Demers (1988) have presented viscometric data for sensitive clays between 0.01-0.20 Nsm^{-2}. These values are 10-200 times the viscosity of water, and thus fit very well the theories and experiments made by Wildemuth and Williams (1985).

2.3 Steady flow with constant height

Steady shear flow with constant height h implies in the two-dimensional case zero acceleration in the direction of flow, the x-direction, as well as in the y-direction. Thus the forces acting on the flow must be in equilibrium in both of these directions at any point x down the slope.

With reference to Fig. 2 these equilibrium conditions will be

$$\sigma_y = (\bar{\rho} - \rho_f)\, g \cos\alpha \;(h - y) + \rho_f g\,(H-y)\cos\alpha + p_a \tag{6}$$

$$\tau_{xy} = (\bar{\rho} - \rho_f)\, g \sin\alpha\,(h - y) - \tau_h \tag{7}$$

for the y- and the x-direction respectively.

Here τ_h = the shear stress acting on the upper boundary (y = h) of the dense flow. The value of τ_h will be discussed later.

The stresses σ_y and τ_{xy} are on the other hand given by the constitutive Eqs. (2) and (4). These two equations are coupled through the effective pressure which thus can be eliminated, giving as a final result the following expression for the velocity gradient.

$$\frac{dv_x}{dy} = \frac{(\rho' g \sin\alpha - \rho_e' g \cos\alpha\tan\varphi)(h-y) - (\tau_h + c)}{\bar{\rho}(m - \nu_2 \tan\varphi)} \tag{8}$$

where $\rho' = \bar{\rho} - \rho_f$

$\rho_e' = \bar{\rho} - \rho_f\,(1 + \Delta u)$

This expression is, however, only valid in regions where the shear stresses acting on the material exceed the shear strength τ_p of the material. This may occur in the lower and upper parts of the flow, within the bounds $0 \le y \le h_1$ and $h_2 \le y \le h$. With reference to Fig. 3 these heights h_1 and h_2 are given respectively by

$$\frac{h_1}{h} = 1 - \frac{\tau_h + c}{gh(\rho' \sin\alpha - \rho_e' \cos\alpha\tan\varphi)} \tag{9}$$

$$\frac{h_2}{h} = 1 - \frac{\tau_h - c}{gh(\rho' \sin\alpha + \rho_e' \cos\alpha\tan\varphi)} \tag{10}$$

For the three different layers the velocity gradient will then be given respectively as:

for $0 \leq y \leq h_1$

$$\frac{dv_x}{dy} = \frac{(\rho' g \sin\alpha - \rho'_e g \cos\alpha \tan\varphi)(h-y) - (\tau_h + c)}{\overline{\rho}(m - \nu_2 \tan\varphi)} \tag{11}$$

for $h_1 \leq y \leq h_2$

$$\frac{dv_x}{dy} = 0 \tag{12}$$

for $h_2 \leq y \leq h$

$$\frac{dv_x}{dy} = -\frac{(\rho' g \sin\alpha + \rho_e g \cos\alpha \tan\varphi)(h-y) - (\tau_h - c)}{\overline{\rho}(m - \nu_2 \tan\varphi)} \tag{13}$$

If the parameters m, ν_2, ρ and Δu are known functions of y, the Eqs (11)-(13) can in principle be integrated. In the present case these parameters are assumed constant, indicating that the flowslide consists of a homogeneous material, and with the excess pore pressure linearly increasing from the upper boundary toward the bed.
Based on these assumptions Eqs (11)-(13) give the following expressions for the flowslide terminal velocity:

for $0 \leq y \leq h_1$

$$v(y) = v_o + 0.5 \frac{g(\rho' \sin\alpha - \rho_e \cos\alpha \tan\varphi) h_1^2}{\overline{\rho}(m - \nu_2 \tan\varphi)} \left[1 - (1 - \frac{y}{h_1})^2\right] \tag{14}$$

for $h_1 \leq y \leq h_2$

$$v = v(h_1) \tag{15}$$

for $h_2 \leq y \leq h$

$$v(y) = v(h_1) - 0.5\frac{g(\rho' \sin\alpha + \rho_e' \cos\alpha \tan\varphi)(h-h_2)^2}{\bar{\rho}(m - v\tan\varphi)}\left[1-(1-\frac{h-y}{h-h_2})^2\right] \qquad (16)$$

where v(0) = slip velocity at the bed. The Equations (14) and (16) satisfy the condition that the velocity gradient at the boundaries of the plug flow are zero. A typical stress diagram and the resulting terminal velocity profile are shown in Fig. 3.

For practical purposes it has been assumed that the velocity profile can be represented by a continuous velocity distribution. For this project a velocity profile consisiting of a sinus-curve and a straight line has been proposed:

$$v(y) = v_1 \sin(\frac{\pi}{2}\frac{y}{h}) - v_2\frac{y}{h} \qquad (17)$$

In Fig. 3 the profile for the equation

$$v(y) = 2.6v(h)\sin(\frac{\pi}{2}\frac{y}{h}) - 1.8v(h)\frac{y}{h} \qquad (18)$$

is shown. Fig. 3 indicates clearly that the theoretical profile fairly well can be replaced by the profile, Eq. (17). One has to bear in mind that the theoretical profile is based on the assumptions that $\bar{\rho}$, m, $\bar{v}$, and Δu are assumed constant during the flow. It thus seems reasonable to substitute the theoretical profile with an approximate profile. The difference between the two is also of less significance due to the fact that the profiles will be integrated.

3. NON-STEADY FLOW

3.1 The momentum equation

To analyse the general non-steady problem the momentum integral equation will be used. As before, the flow is assumed to be two-dimensional, but now the flow velocity can vary also with x and t, i.e.

$$v_x = v_x\,(x,\ y,\ t) \qquad (19)$$

and the height h is given as

$$h = h\,(x,\ t) \tag{20}$$

By considering the flow at any instant through the control volume shown in Fig. 4, the momentum equation for the flow direction takes the form

$$\frac{\partial}{\partial t}\int_o^h \bar{\rho} v_x dy + \frac{\partial}{\partial x}\int_o^h (\bar{\rho} v_x)\, v_x dy = F_x \tag{21}$$

The control-volume is fixed in x, but its height h is allowed to vary in such a way that its upper surface at all times coincide with that of the dense flow. This is indicated by the fact that the two partial differential operators $\partial/\partial t$ and $\partial/\partial x$ both operate on the two integrals as a whole.

The first of the two integrals on the left hand side represents the rate of change of momentum of the mass actually within the control volume at any particular time t while the second considers the net transport per unit time of momentum out of the control volume at the same instant.

The force F_x on the right hand side of the equation is the component in the x-direction of the resultant of all the forces acting on the control-volume. The infinitesimal length dx of the control volume is common to all the three terms of the equation and is therefore divided out.

For the steady flow with constant height, h, as discussed in Section 2.3, we have that $\partial/\partial t = \partial/\partial x = 0$, making each term on the left hand side of Eq. (21) identical to zero, i.e.

$$F_x = 0 \tag{21a}$$

In the later discussion of the boundary conditions at the bed, variations in the height are considered insignificant, and Eq. (21) thus takes the form

$$\frac{\partial}{\partial t}\int_o^h \overline{\rho} v_x dy = F_x \tag{21b}$$

3.2 The acting forces

The forces acting on the control volume are indicated on Fig. 4. In the x-direction these are in sum:

$$F_x = (\overline{\rho}-\rho_f) g \sin\alpha \; h - \frac{\partial}{\partial x}\int_o^h \sigma_x dy + p_1 \frac{\partial h}{\partial x} - (\tau_h + \tau_o) \tag{22}$$

where the first term is the driving force due to gravity, while the second, third and fourth terms represent the forces due to the stresses acting on the vertical, the top and the bottom surfaces of the control-volume respectively.

For the approximations made in this case, accelerations in the y-direction can be neglected, and thus the normal stress σ_y at any level y is still given by Eq. (6):

$$\sigma_y = (\overline{\rho} - \rho_f) g\cos\alpha \; (h-y) + \rho_f \; g(H-y)\cos\alpha + p_a \tag{6}$$

The constitutive Equations (1) and (2) will give that

$$\sigma_x - \sigma_y = -\nu_1 \overline{\rho} \frac{\partial v_x}{\partial y} \tag{23}$$

which together with Eq. (6) finally gives

$$\sigma_x = (\overline{\rho}-\rho_f) g\cos\alpha (h-y) + \rho_f g\cos\alpha (H-y) + p_a - \nu_1 \overline{\rho} \frac{\partial v_x}{\partial y} \tag{24}$$

The pressure p_1 on the upper control surface is given by

$$p_1 = \rho_f \; g\cos\alpha(H-h) + p_a \tag{25}$$

while the shear stress τ_h on the same surface will be discussed later.

The shear stress $\tau_o \equiv \tau_{xy/y=0}$ is also left to a later discussion.

With Eqs (24) and (25) in Eq. (22) the resultant force in the x-direction will finally be found to be given as:

$$F_x = (\bar{\rho}-\rho_f) g \sin\alpha h - (\tau_h+\tau_o) - (\bar{\rho}-\rho_f) g \cos\alpha h \frac{\partial h}{\partial x} + \frac{\partial}{\partial x} \int_o^h \bar{\rho} v_1 \frac{\partial v_x}{\partial y} dy \quad (26)$$

Here h, v_x and H are all functions of x. With an exact or assumed distribution of v_x in the y-direction, the integration in the last term on the right hand side above may be carried out.

The velocity-distribution given by Eq. (17) has earlier been shown to give a close approximation to the theoretical profile calculated for the steady flow with constant height h.

Although Eq. (17) may be expected to give a less satisfactory approximation in the non-steady state case, the integration of the profile in the different terms of the momentum equation makes divergencies less significant. The velocity distribution given by Eq. (17) is thus assumed valid also in the non-stedy case, i.e.

$$v(y) = v_1 \sin\left(\frac{\pi}{2}\frac{y}{h}\right) - v_2 \frac{y}{h} \quad (17)$$

The last term in the expression for F_x will then be

$$\frac{\partial}{\partial x} \int_o^h \bar{\rho} v_1 \frac{\partial v_x}{\partial y} dy = \bar{\rho} v_1 \left(\frac{2}{\pi} v_1 - \frac{1}{2} v_2\right) \frac{\partial h}{\partial x} \quad (27)$$

The parameters $\bar{\rho}$ and v_2 are assumed constant.

3.3 The change of momentum terms

The left hand side of the momentum Eq. (21) can now be calculated to be

$$\frac{\partial}{\partial t}\int_o^h \bar{\rho} v_x dy + \frac{\partial}{\partial x}\int_o^h (\bar{\rho} v_x) v_x dy =$$

$$= \bar{\rho}\left\{\frac{\partial}{\partial t}\left\{\frac{2h}{\pi} v_1 - \frac{1}{2} v_2 h\right\} + \left\{\frac{\partial}{\partial x}\left\{\frac{h}{2} v_1^2 - \frac{8h}{\pi^2} v_1 v_2 + \frac{h}{3} v_2^2\right\}\right\}\right\} \tag{28}$$

The momentum equation for the general problem of non-steady flow with varying height h and with a velocity-distribution assumed given by Eq. (17) will thus take the form

$$\bar{\rho}\frac{\partial}{\partial t}\{\frac{2h}{\pi} v_1 - \frac{h}{2} v_2\} + \bar{\rho}\frac{\partial}{\partial x}\{\frac{h}{2} v_1^2 - \frac{8h}{\pi^2} v_1 v_2 + \frac{h}{3} v_2^2\} =$$

$$= (\bar{\rho} - \rho_f) g \sin\alpha h - (\tau_h + \tau_o) - (\bar{\rho} - \rho_f) g \cos\alpha h \frac{\partial h}{\partial x} + \tag{29}$$

$$+ \bar{\rho} v_1 \{\frac{2}{\pi} v_1 - \frac{1}{2} v_2\} \frac{\partial h}{\partial x}$$

3.4 Kinematic condition for the upper boundary

For the approximations made not only the acceleration in the y-direction but also the corresponding velocity in this direction can be neglected. This means that

$$v_y \approx 0 = \frac{Dh}{Dt} = \frac{\partial h}{\partial t} + v_x \frac{\partial h}{\partial x} \tag{30}$$

Thus

$$\frac{\partial h}{\partial t} = -v_h \frac{\partial h}{\partial x} = -[v_1 - v_2] \frac{\partial h}{\partial x} \tag{31}$$

This makes it possible to substitute for $\partial h/\partial t$ in the momentum equation, but terms including $\partial v_1/\partial t$ and $\partial v_2/\partial t$ will still remain.

3.5 The equation of continuity

In the present case the masses involved are assumed incompressible, and the mass balance for the flow through the control volume is therefore secured by the equation of continuity in the following form:

$$\frac{\partial}{\partial x}\int_{o}^{h} v_x dy + \frac{\partial h}{\partial t} = 0 \tag{32}$$

where $\partial h/\partial t$ is the velocity in the y-direction of the upper boundary.

Substituting for v_x from Eq. (17) and for $\partial h/\partial t$ from Eq. (31) continuity will finally be expressed by

$$\frac{\partial}{\partial x}\{\frac{2h}{\pi}v_1 - \frac{h}{2}v_2\} = \{v_1 - v_2\}\frac{\partial h}{\partial x} \tag{33}$$

or, after rearranging

$$\frac{1}{h}\frac{\partial h}{\partial x} = \frac{\frac{\partial}{\partial x}\{\frac{2}{\pi}v_1 - \frac{1}{2}v_2\}}{\{(1-\frac{2}{\pi})v_1 - \frac{1}{2}v_2\}} \tag{34}$$

linking h, v_1 and v_2 and their derivatives with respect to x.

3.6 The final system of equations

The mathematical problem in the general case has 3 unknown functions of the 2 variables, time t and coordinate x,

$$h\,(x,t);\ v_1(x,t);\ v_2(x,t)$$

As the momentum equation, Eq. (29) has been integrated in the y-direction, this coordinate no longer appears, leaving a one-dimensional equation in the coordinate x.

After rearranging, Eq. (29) takes the form

$$\begin{aligned}&\bar{\rho}\frac{\partial}{\partial t}\{\frac{2}{\pi}hv_1 - \frac{1}{2}hv_2\} + \bar{\rho}\frac{\partial}{\partial x}\{\frac{1}{2}hv_1^2 - \frac{8}{\pi^2}hv_1v_2 + \frac{1}{3}hv_2^2\} + \\ &\quad + \{(\bar{\rho}-\rho_f)ghcos\alpha - \bar{\rho}v_1(\frac{2}{\pi} - \frac{1}{2}v_2)\}\frac{\partial h}{\partial x} - \\ &\quad - (\bar{\rho}-\rho_f)gsin\alpha h + (\tau_h + \tau_o) = 0\end{aligned} \tag{35}$$

In summary this equation together with the equation of continuity, Eq. (34), and the kinematic condition at the upper boundary, Eq. (31), constitute the necessary 3 differential equations for the 3 unknown functions h, v_1 and v_2.

The shear stresses τ_h and τ_o will be given by separate equations discussed and presented in the following sections.

An additional equation has to be introduced if a slip velocity will develop. This velocity will also be a function of both time and distance. The existence and the calculation of a slip velocity will be discussed in Section 5.3.

4. THE BOUNDARY CONDITIONS AT THE UPPER BOUNDARY

Full-scale experiments with snow avalanches have shown that in the steep part of the avalanche path, the dense flow is a short distance ahead of the turbidity current. The turbity current is therefore assumed to be generated by shear stresses at the upper boundary of the dense flow.

Norem et al (1989) proposed to assume these shear stresses to be comparable with the stresses acting on a solid moving into a more or less undisturbed fluid. This assumption can be justified when the avalanche has a small thickness to length ratio and if currents and effects of long surface waves can be neglected. For such conditions the shear stresses estimated by boundary layer theory over flat plates were proposed.

For turbulent flow over a flat rough plate the non-dimensional shear stress at any point x, measured from the leading edge of the plate, along the plate is defined by the equation proposed by Schlichting (1966).

$$\tau/\rho v^2 = \frac{1}{2}[2.87+1.58\log(x/k)]^{-2.5} \qquad (36)$$

where ρ = the density of the fluid above the plate flow
v = the undisturbed fluid velocity

k = the roughness of the plate

In the present context it is assumed that the density can be selected as the density of the mixed fluid above the dense flow. This is probably higher than the fluid density because of high particle content in the boundary layer. The flow velocity is the velocity at the upper boundary at each element.

The roughness length k has yet to be determined. Bagnold (1962) considered ripples forming on the beds of sand or silt and concluded that k would be likely to lie somewhere between the ripple length and the grain size. This has led us to assume that k will be in the range 0.01-0.1 m.

It is clear from the graph in Fig. 5 that the highest stresses are found close to the front, where the thickness of the boundary layer is small. With increasing distance from the front, $x/k \geq 6000$ or $x \approx 300$ m, the shear stresses are reduced to an almost constant level.

The authors have no knowledge of any recordings of these boundary shear stresses for any kind of avalanches. NGI has, however, experience from recording impact pressures from snow avalanches. These recordings show that the highest impacts from the turbidity currents are found close to the front of the avalanche (Norem et al, 1985-1989). This indicates that the highest boundary stresses also should be found close to the front of the slide.

The boundary shear stresses may also be averaged over the slide length L, and the averaged shear stress, τ', becomes:

$$\tau'/\rho v^2 = 0.5 \left[1.89 + 1.62 \, (L/k) \right]^{-2.5} \qquad (37)$$

The plots in Fig. 5 show that these stresses fall rapidly off to a more or less constant value for L/k greater than 4000.

The importance of the shear stress on the upper boundary depends on the flow height, the length of the slide and the value of the rougness length, k. Generally, the boundary conditions are more important for minor slides than for major slides and if k should be significantly above

0.1 m.

As a rule the turbidity currents generated by submarine slides draw more attention than the slides themselves. The turbidity currents may show substantial flow heights and have impressively long run-out distances. They must be a result of the shear stresses acting on the upper boundary of the slide as well as the turbulent transport of mass up into the turbidity current caused by these stresses.

The mechanism by which the turbidity currents are generated seems to have been given only little attention in the literature. Most known models are based on assumptions that the entrainment is a function of the distance from the head of the avalanche.

A more correct physical approach is, probably, to estimate the entrainment as a function of the shear stresses at the boundary. This will be in accordance with theories developed for drifting sand in wind, drifting snow and bed load formulas for sediment transport in rivers. A method by which the magnitude of the mass flux through the upper boundary can be estimated, have yet to be established.

The mass flux through the upper boundary is however assumed to have minor importance for the flow of the dense part, but to have significant importance for the flow of the turbidity part of submarine slides.

5. BOUNDARY CONDITIONS AT THE BED

5.1 Assumptions made to model the properties at the bed

The boundary conditions at the bed are more complex to represent than the previously discussed conditions at the upper boundary. While the condition at the upper face was shown mainly to depend on the velocity of the upper face of the dense slide, the conditions at the bed will be strongly dependent on the material properties of the bed as well as of the dense slide. A good modelling of the conditions at the bed will thus depend on a good understanding of the physical processes that take place

there. All existing numerical models assume that flowslides are flowing on fixed beds. Sassa (1988) has however, presented some ideas for the pore pressures variations within the bed while the flowslides pass over, thus giving necessary physical assumptions for erosion to take place.

A flowslide is assumed to flow on an inclined slope, Fig. 6. Any change of the volume of the element is considered to happen at the lower boundary and the flow height above the boundary is assumed to be constant.

The conditions at the bed may be divided into two groups according to whether the dense flow slides over:

1. Non-erosive beds, i.e. beds in which the plasticity shear strength exceeds the stress demanded by the dynamics of the flowslide, or

2. Erosive beds, i.e. beds with plasticity shear strengths less than the shear stress demanded by the flow in Group 1. and consequently apt to erode and entrain masses into the dense slide.

5.2 Non-erosive bed

Nishimura (1990) carried out model experiments with coarse grained snow particles flowing down an inclined chute. The bed for the experiment consisted of either polyethylene film, glued snow particles or sandpaper having the same roughness as the snow particles. Fig. 7 shows the recorded velocity profiles, indicating that a slip velocity is only existing when the roughness parameter, represented by the grain diameter, is less than the grain diameter in the flowing material.

Most submarine slides flow over beds consisting of almost the same type of material as the material involved in the slide. It is thus reasonable to assume that no slip will occur in real slides. In model experiments, however, the roughnes of the boundary may differ considerably from that of the flowing material, making a slip velocity more likely to occur, Fig. 7.

For a one-dimensional flow with constant h all derivatives with respect to x will be zero, and thus eqs (21) and (26) will be reduced to:

$$\bar{\rho}\frac{d}{dt}(\bar{v}h) = \rho' gh\sin\alpha - (\tau_h + \tau_b) \tag{38}$$

where

$$\bar{v} = v_o + \frac{1}{h}\int_o^h v_x dy = v_o + \overline{v_h - v_o} = \textit{the average velocity} \tag{39}$$

τ_b = shear stress at the lower boundary

τ_h = shear stress at the upper boundary

The shear stress at the bed, τ_b , can be estimated by either of the following equations:

1. When a non-slip velocity condition exists the shear stress may be calculated by the constitutive equations for the flowing material.

2. When a slip velocity develops the shear stress at the bed is only defined by the shear stresses within the boundary layer. In this case Norem et al. (1989) assumed the shear stress to be represented by the expression:

$$\tau_i = \rho_e' \; gh \cos\alpha \tan\varphi_b + \rho s \; v_o \tag{40}$$

where

τ_i = shear stress at the bed interface

φ_i = Coulomb friction angle at the bed interface

s = a roughness parameter

The acceleration excluding the slip velocity is given by the forces acting on the control volume, the shear stress at the bed given by the constitutive equations and the shear stress at the upper boundary.

$$\bar{\rho}h\frac{d}{dt}(\overline{v_h - v_o}) = \rho' gh\sin\alpha - \rho'_e gh\cos\alpha \tan\varphi - \bar{\rho}(m - v_2\tan\varphi)\frac{dv_x}{dy}\Big|_{y=0} - \tau_h \tag{41}$$

If the shear stress at the boundary is less than the shear stress in the flowing material, a slip velocity will develop and Eqs (38), (39) and (41) yield the following differential equation for the slip velocity

gradient with time:

$$\frac{dv_o}{dt} = \frac{1}{\bar{\rho}}[\rho_e' g(\tan\varphi - \tan\varphi_b)\cos\alpha + \bar{\rho}(m - \nu_2\tan\varphi)\frac{dv_x}{dy}|_{y=0} - \bar{\rho}\frac{sv_0}{h}] \quad (42)$$

Equation (40) indicates that the slip velocity is dependent on the difference of the friction parameters, φ and φ_b, the relative importance of the kinetic parameters m and s. The main contribution comes probably from the first term on the right hand side, showing that a significant slip velocity may only develop if the friction coefficient at the bed is less than the friction coefficient of the granular material.

5.4 Erosive bed

If the bed consists of a soft bed the transferred shear stresses may exceed the shear strength of the bed material. In this case erosion of the bed may occur. The granular material of the bed may be assumed to show a visco-plastic behaviour represented by the equation:

$$\tau_b = (\bar{\rho} - \rho_f\ (1 + \Delta u_b\ ))\ gh\ \cos\alpha\ \tan\varphi_b \quad (43)$$

where τ_b = the shear strength of the bed material
φ_b = Coulomb friction angle of the bed material
Δu_b = excess pore pressure in the bed material

When erosion takes part there is not assumed to be any slip velocity. It is also assumed that the eroded particles adjust themselves to the original velocity profile. The eroded particles will thus serve to increase the flow height gradually and be accellerated to a velocity defined by the velocity profile (Eq. 17), Fig. 6.

The equation of momentum based on these assumptions will be:

$$\bar{\rho}\frac{d}{dt}(\bar{v}h) = \frac{\bar{v}}{v_h}\bar{\rho}(h\frac{\partial v_h}{\partial t} + v_h\frac{\partial h}{\partial t}) + 0(\frac{\partial \bar{v}h}{\partial x}) = \rho' gh\sin\alpha - (\tau_o - \tau_p) \quad (44)$$

All gradients in the x-direction are considered to be insignificant

compared to the other terms, and the expression $(\delta\bar{v}h/\delta x) \approx 0$.

Equations (40) and (41) make it possible to develop a differential equation for the increase of flow height with time, i.e. the rate of erosion.

$$\frac{\partial h}{\partial t} = \frac{1}{\overline{\rho v}}[ghcos\alpha(\rho_e'tan\varphi-((\bar{\rho}-\varrho_f(1+\Delta u_b))tan\varphi_b)+\bar{\rho}(m-\nu_2 tan\varphi)\frac{dv_x}{dy}|_{y=0}-\tau_h] \quad (45)$$

The paranthesis of the right hand side of eq. 45 consists of three terms, each of them dependent on:

(1) the differende of the apparanet Coulumb friction for respectively the flowing material and the bed material
(2) the viscous shear stress at the bed
(3) the shear stress at the upper boundary

A typical submarine flowslide is assumed to have the following parameter values.

Flow height: 2 m
Flow length: 400 m
Veolicity: 15 m/s
Friction angle, tan ϕ : 27°
Shear and normal viscosity: 0.1 and 0.17 Pas.
Shear stress at upper boundary: $2 \cdot 10^{-3}\ \rho v^2$

The calculated values for the three terms and the resulting erosion are shown in fig. 8. The two axes are the ratio of the apparanet Coulomb friction for the bed and the flowing material respectively, and the ratio erosional depth to the flowing height.

The most dominant terms of eq 45 are the first and the last terms, which have opposite signs. Fig. 8 indicates that no erosion will occur unless there is a significant difference in the apparant Coulomb frictions. For ratios below 0.75 - 0.85 erosion caused by the flowslides may become an substantial part of the mass involved in the slide. Such a difference in the apparent Coulomb frictions may be explained as follows:

1. The properties of the bed material along the path is different of that material involved in the flowslide.

2. When passing over the bed, the flowslide will cause a sudden increase in the normal and shear stresses at the bed. This increase may generate high excess pore pressures and thus reduce the shear strength of the bed material. This effect has been discussed by Sassa (1988).

6. CONCLUSIONS

The report presents ideas and expressions in an attempt to describe physically and mathematically the flow of the dense part of submarine flowslides. It is the hope of the authors that the physics of the flow is fairly well described, but it is still necessary to do a parametric study, and to do model and full-scale experiments to predict the flow of such slides more accurately.

The material of the dense part of submarine flowslides are assumed to behave as a homogeneous, visco-plastic material. The presented constitutive equations fit well into laboratory experiments of granular materials, and probably also represent fairly well the dynamic behaviour of silt particles having water as the interstitial fluid, and to understand the long run-out distance submarine slides are the excess pore pressure, which can obtain substantial values due to the process of liquefaction and to velocity gradients in the flowing material.

Model experiments on granular flow indicate that there exist velocity gradients in the flow, and that will probably also be the case in real avalanches. The calculations are based on assumptions that the velocity profile can be approximated with a combination of a sinus and a linear profile. The approximate profile is very close to the estimated theoretical profile.

The velocity profile is depth-averaged and the equations for non-steady flow are then developed based on classical hydro dynamical theories. The presented equations seem to describe the two-dimensional flow fairly correct, if the basic assumptions, that the flowing material is

homogeneous and have a visco-plastic behaviour, is true. This has still to be proven.

The study shows that the physical processes at the boundaries are very important for calculating the flow of the slides. The shear stresses at the upper boundary are assumed to be comparable with the shear stresses in the turbulent boundary layer along a flat plate. Previously rough estimates indicate that these stresses may be as high as one third of those at the bed. Obviously, there is also mass transport from the dense flow to the turbidity current above. This mass flux have probably only minor significance for the flow of the dense part of the slide.

The boundary conditions at the bed are more complex to represent than the conditions at the upper surface. The main factors to take into account are the material properties of the bed as well as those of the dense slide.

There will be no erosion if the shear strength of the bed material exceeds the stress required by the dynamics of the flowslide. In this case there will be no slip velocity if the friction of the bed is equal or higher than the internal friction of the flowing material. In the other case a slip velocity is likely to occur.

Erosion may take place if the tranferred shear stresses exceed the shear strength of the bed material. This may be the case if the slide flows over very soft sediments or high excess pore pressures are generated inside the bed by the sudden increase of normal and shear stresses. It is assumed that eroded particles will serve to increase the flow height and be accelerated to a velocity defined by the velocity profile.

The presented equations for the development of a slip velocity and the erosion depth is a first attempt to describe these processes mathematically. The authors are well aware that more theoretical and experimental research has to be carried out. It is, however, the hope of the authors that these equations represent a step forward to a better understanding of erosion caused by slides. This aspect is very important when evaluating the safety of f.i. oil pipelines, electrical cables and other seabed installations. The entrainment of mass caused by erosion is also found to have a significant importance on the velocity and run-out distance of submarine flowslides.

The presented ideas make it possible to reprogramme the NGI numerical avalanche model based on a fixed bed with no slip velocity. NGI will look for the possibilities to do this reprogramming in order to develop a model which covers several types of natural avalanches.

Acknowledgement

The preparation of this report is a part of the NGI-project on submarine slides. The project is financed by the oil companies Saga Petroleum and Petrobras, the Royal Norwegian Council for Scientific and Industrial Research, The French - Norwegian Foundation for Scientific Research and Norwegian State Power Board. The authors wish to thank the supporting agencies for their kind support.

REFERENCES

Bagnold, R.A. (1954)
Experiments on a gravity-free dispersion of large solid spheres in a Newtonian fluid under shear.
Proceedings of the Royal Society of London, Ser A225, pp. 49-63.

Bagnold, R.A. (1962)
Auto-suspension of transported sediment: turbidity currents.
Proceedings of the Royal Society of London. Ser. A 265, pp. 315-19.

Criminale, W.O.Jr., Ericksen and Filby, G.L. (1958)
Steady shear flow of Non-Newtonian Fluids.
Archive Rat. Mech Anal 1, 410-417, 1958.

Edgers, L. and Karlsrud, K. (1982)
Soil flows generated by submarine slides. Case studies and consequences.
International Conference on the Behaviour of Offshore Structures, 3.
BOSS'82. Cambridge, Mass. 1982. Proceedings, Vol. 2, pp. 425-437.

Hungr, O., and Morgenstern (1984)
High velocity ring shear tests on sand.
Géotechnique, 34, pp. 415-421.

Hutchinson, J.N. (1986)
A sliding-consolidation model for flow slides.
Canadian Geotechnical Journal, 23, pp. 115-126.

Hutchinson, J.N., and Bhandary, R.K. (1971)
Undrained loading a fundamental mechanism of mudflows and other mass movements.
Géotechnique, 21, pp. 353-358.

Irgens, F. (1988)
A continuum model of granular media and simulation of snow avalanche flow in run-out zones.
Pres. at XVII. ICTAM Grenoble 1988.

Kummeneje, O., and Eide, O. (1961)
Investigations of loose sand deposits by blasting.
NGI-publ. no. 45.

Locat, J., and Demers, D. (1988)
Viscosity, yield stress, remolded shear strength, and liquidity index relationships for sensitive clays.
Canadian Geotechnical Journal, 25, pp. 799-806.

Nishimura, K. (1990)
Studies on the fluidized snow dynamics (thesis).
Inst. of Low Temp. Science, Sapporo.

Norem, H., Irgens, F., and Schieldrop, B. (1987)
A continuum model for calculating snow avalanche velocities.
Proceedings of Avalanche Formation, Movements and Effects, Davos, 1986.
IAHS Publ., 162, pp. 363-379.

Norem, H., Tronstad, K., Kristensen, Kr. (1985-1989)
The Ryggfonn project. Avalanche data from the 1983-1989 winters.
Norwegian Geotechnical Institute, Reports 58120-6, -7, 8, 10, 11, 13 and -15.

Norem, H., Irgens F., and Schieldrop, B. (1989)
Simulation of snow avalanche flow in run-out zones.
Annals of Glaciol. no. 13.

Norem, H., Locat, J. and Schieldrop, B. (1989)
An approach to the physics and the modelling of submarine flowslides.
Norwegian Geotechnical Institute, Report 522090-2. Also to be published in Marine Geotechnology, Vol. 9, No. 2 1991.

Sassa, K. (1988)
Geotechnical model for the motion of landslides.
Proceedings of the Fifth Int. Symp. on Landslides, Lausanne. C. Bonnard, ed., vol. 1, pp. 37-56.

Savage, S.B. (1983)
Granular flows down rough inclines. Review and extensions.
Mechanics of Granular Materials, Ed.; Jenkins and Satake, pp. 261-282
Elsevier.

Savage, S.B., and Sayed, M. (1984)
Stresses developed by dry cohesionless granular materials in an annular shear cell.
J. Fluid Mech. vol. 142, pp. 391-430.

Schlichting, H. (1968)
Boundary Layer Theory.
McGraw Hill.

Wildemuth and Williams (1985)
A new interpretation of viscosity and yield stress in dense slurries.
Rheol. Acta 24: 75-91.

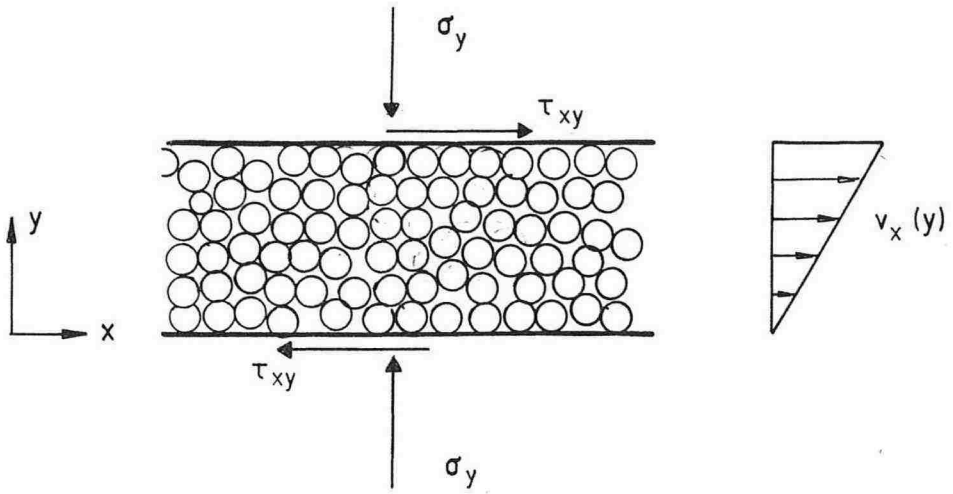

Fig. 1: Definition of normal and shear stresses and the velocity distribution.

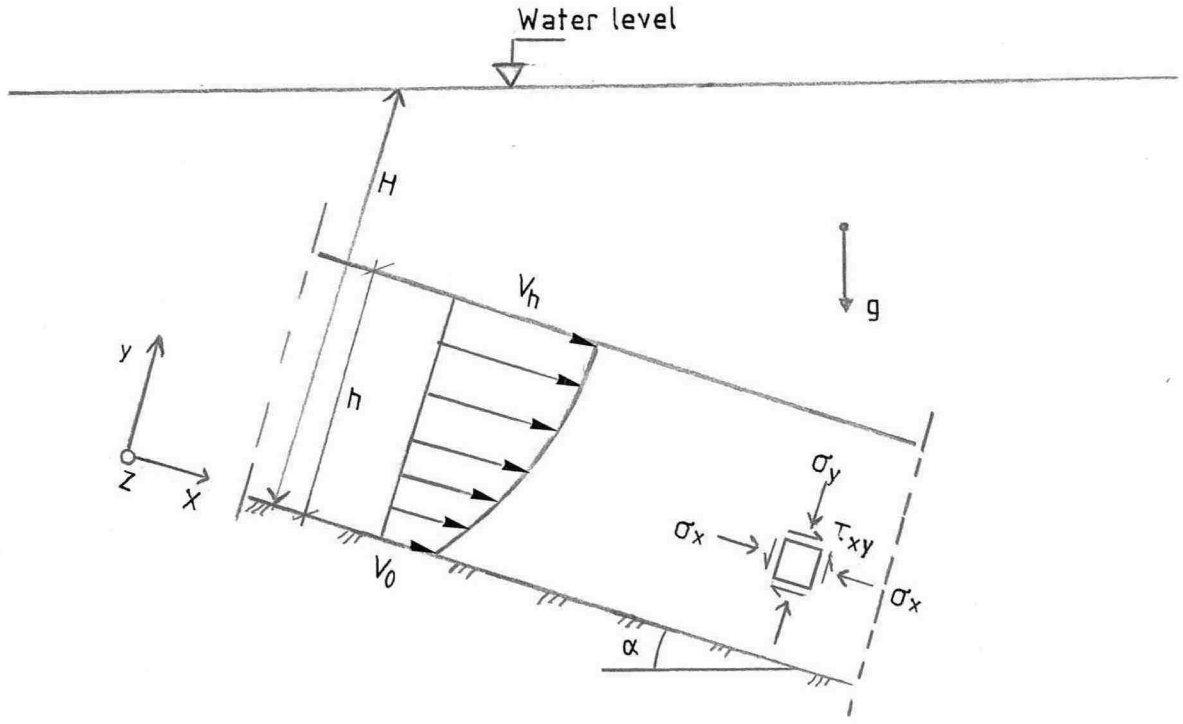

Fig. 2: Definition of steady geometry.

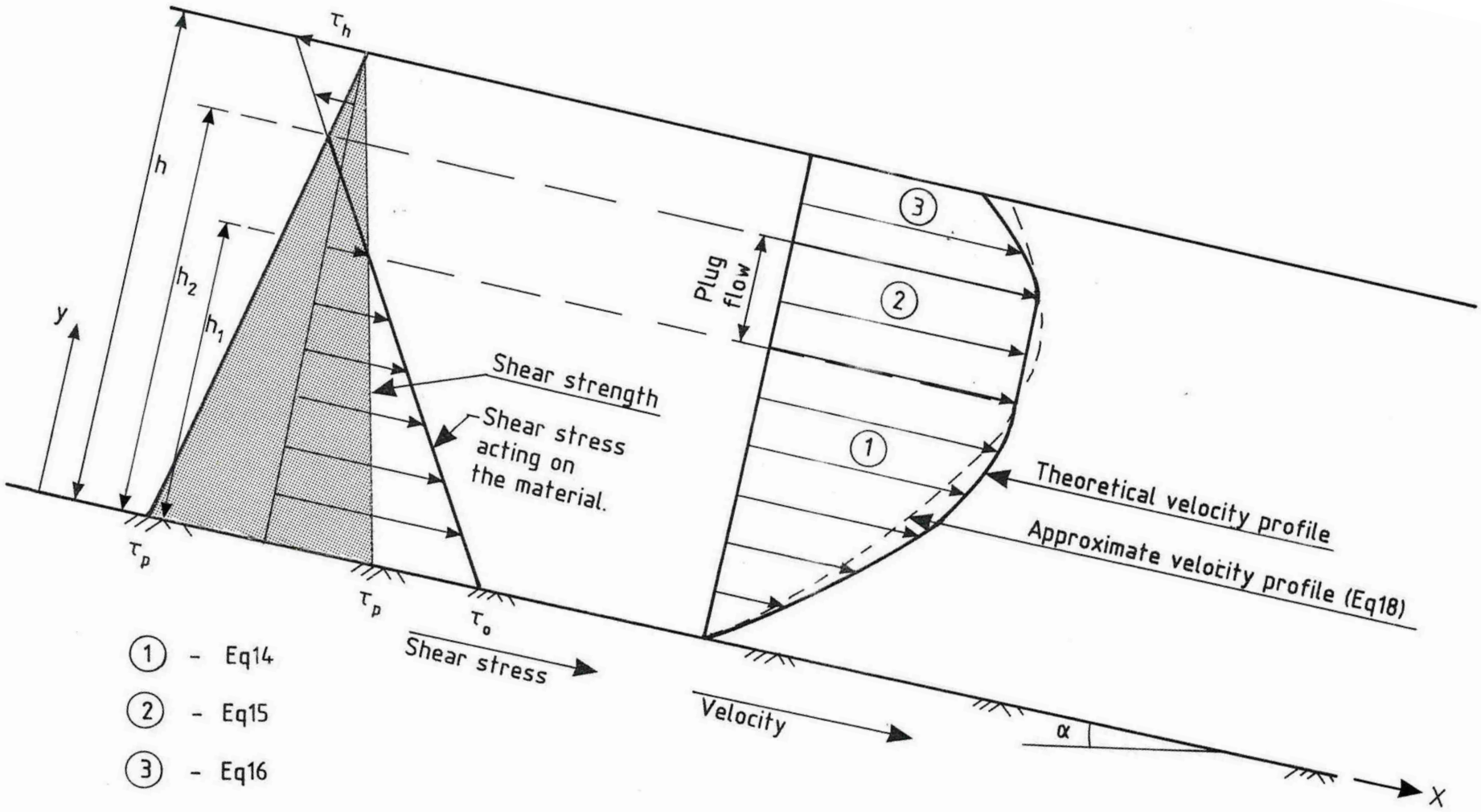

Fig. 3. Shear stress distribution, the resulting theoretical velocity profile for the terminal velocity, and approximate velocity profile.

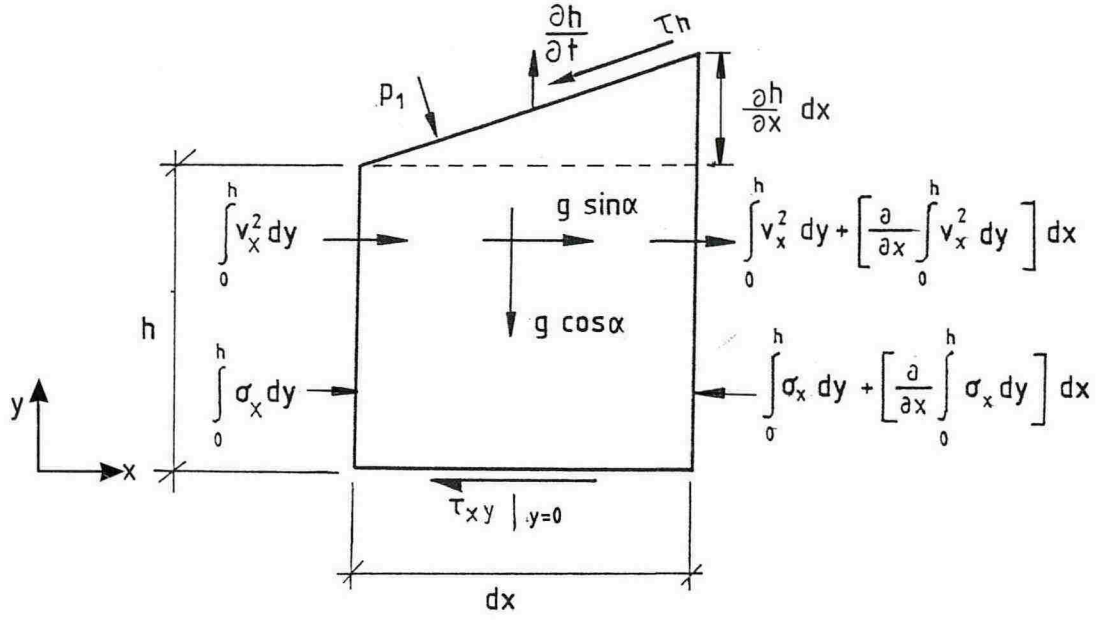

Fig. 4 Differential control volume

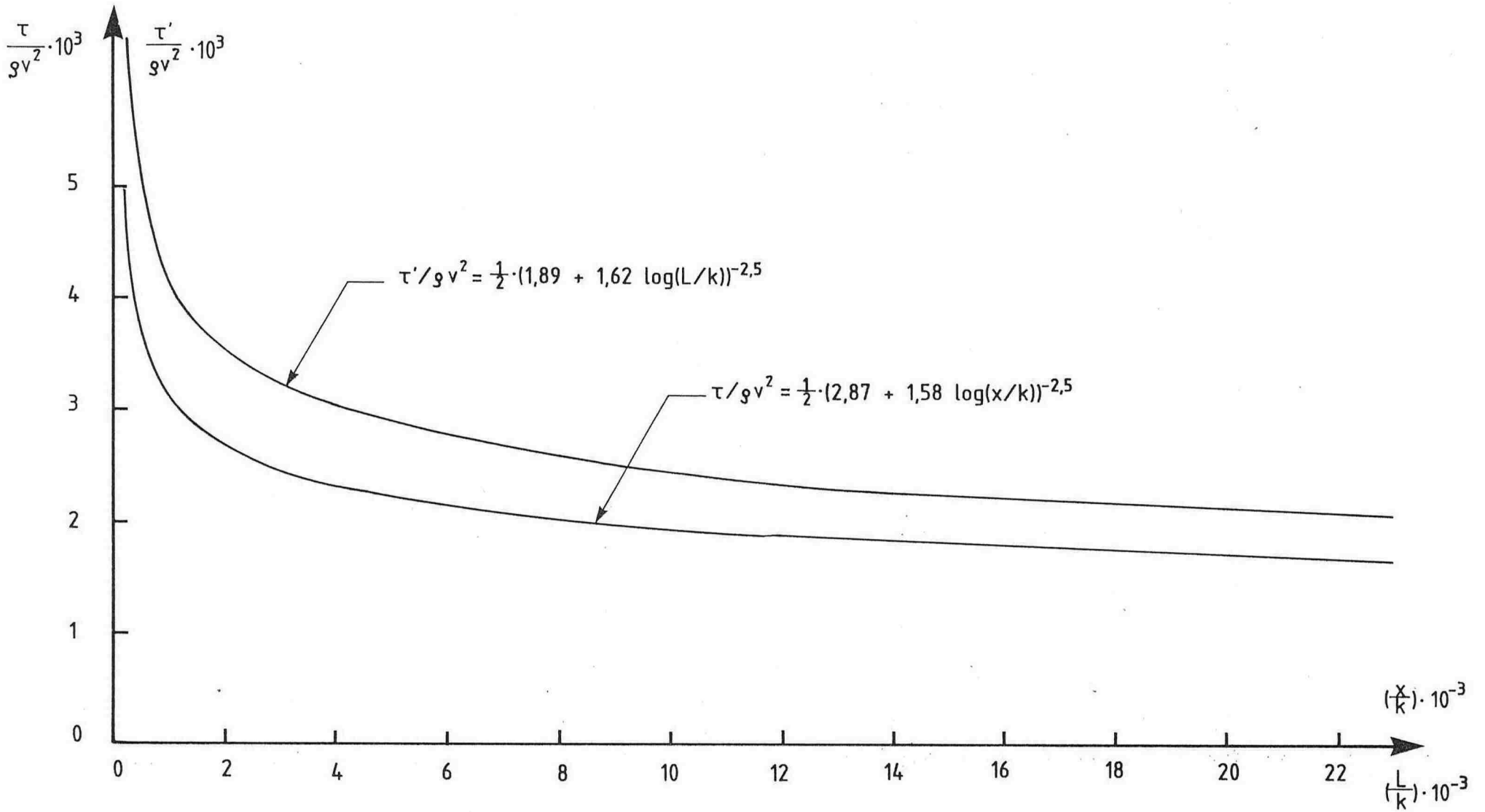

Fig. 5: Non-dimensional boundary shear flow for a rough flat plate.

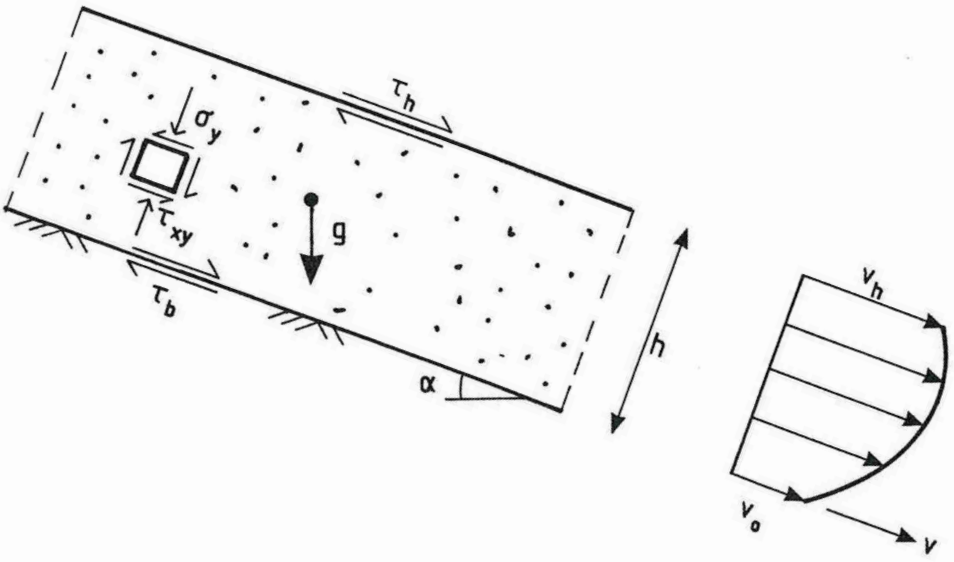

a) Development of slip velocity on a fixed, smooth bed surface.

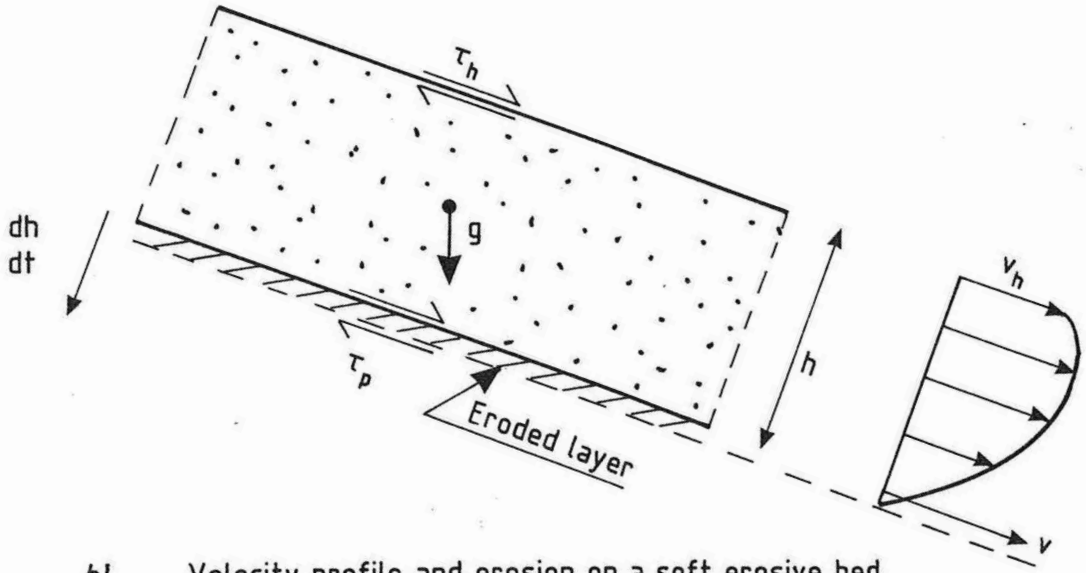

b) Velocity profile and erosion on a soft erosive bed.

Fig. 6. Boundary stresses and velocity profiles for submarine flowslides.

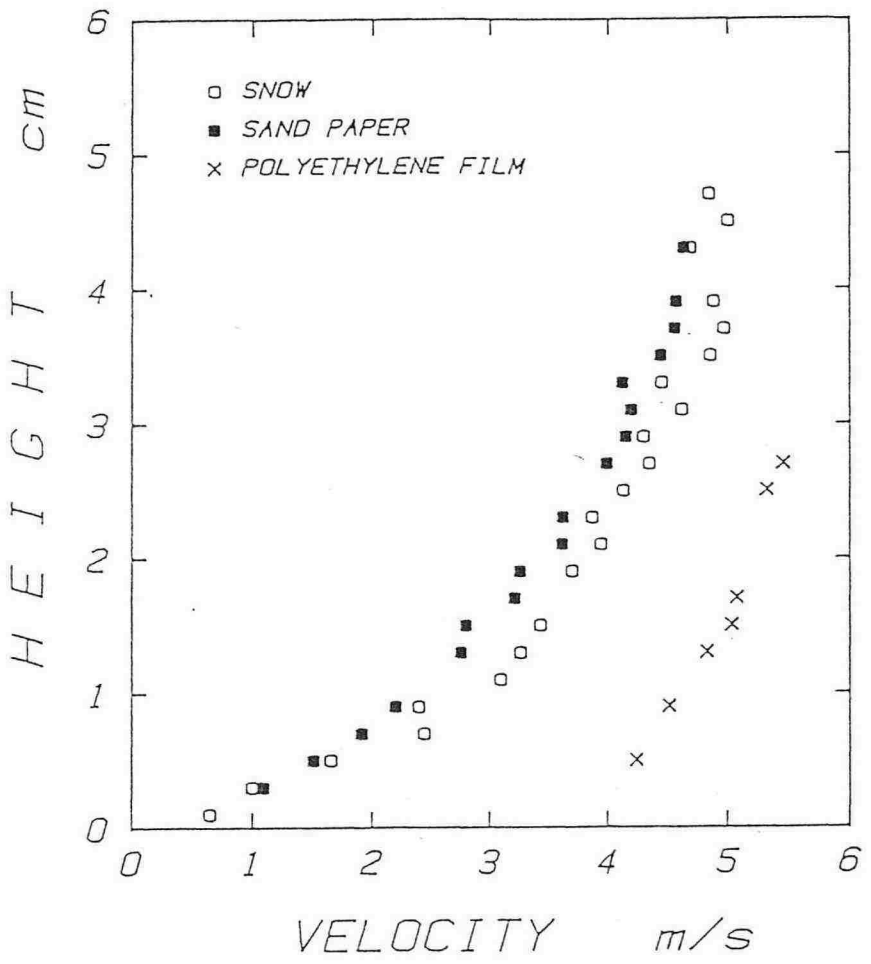

Fig. 7 Velocity profiles of the snow flow on various floor conditions. (Nishimura 1990)

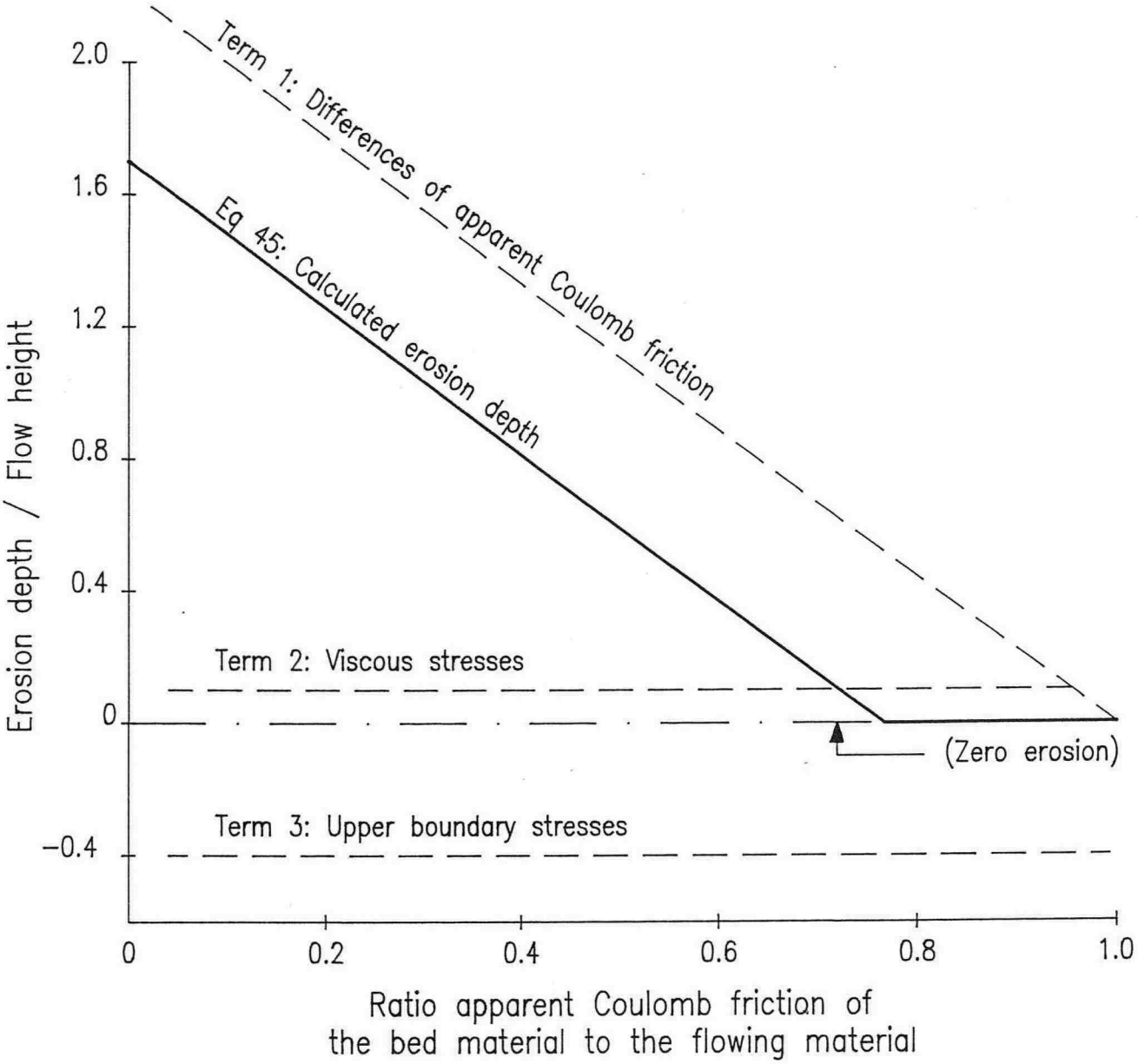

Fig. 8: Calculated erosion depth for a typical submarine flowslide and the individual effect for each of the three physical processes that contributes to erosion.

C:\ACAD386\TEGNING\FLOW